Research Article

Sattaru Gouthamsri, Kommu Jaya Rao*, Malla Ramanaiah*, Keloth Basavaiah

Combustion-mediated sol-gel preparation of cobalt-doped ZnO nanohybrids for the degradation of acid red and antibacterial performance

https://doi.org/10.1515/chem-2023-0129 received May 26, 2023; accepted September 11, 2023

Abstract: The present study explores the combustion-mediated sol-gel preparation of the cobalt-doped ZnO (Co/ZnO) nanohybrids. The characterization results of as-prepared samples were investigated using analytical instruments like FTIR, XRD, XPS, SEM, UV-Vis DRS, BET, and TGA. The doping of cobalt into ZnO was achieved at a lower particle size (21.3 nm) than the pure ZnO (29.6 nm). We observed that the Co-doped ZnO grain size seems to be in abundance and diversity than that of the undoped ZnO. Further examination was carried out with photocatalytic degradation of acid red (AR) dye under visible light illumination and antibacterial performance over Spingomonous pausimobilis and Streptococcus pyrogenes to assess the catalytic performance of the prepared Co/ZnO nanohybrid. The photocatalytic degradation results from the optimum reaction conditions are 150 mg of catalyst loading, pH 2, and 10 ppm of initial AR dye concentration, and the complete degradation of AR dye in 120 min. The antibacterial performance of the Co/ZnO nanohybrid was measured and was found to be 25 and 16 mm for S. pausimobilis and S. pyrogenes, respectively, with respect to the control chloramphenicol.

Keywords: cobalt doped ZnO, acid red dye, visible light illumination, antibacterial performance

Graphical abstract

Abbreviations

Co/ZnO cobalt-doped ZnO XRD X-ray diffraction

SEM scanning electron microscope

FTIR Fourier transform infrared spectroscopy

XPS X-ray photoelectron microscope
TGA thermogravimetric analysis
DRS diffuse reflectance spectroscopy
BET Brunauer–Emmett–Teller

Sattaru Gouthamsri: AU Trans-Disciplinary Research Hub, Andhra University, Visakhapatnam-530003, India; Department of Chemistry, Aditya Institute of Technology and Management, Tekkali-532201, India Keloth Basavaiah: Department of Chemistry, Andhra University, Visakhapatnam-530003, India

1 Introduction

Transparent semiconductors containing conductive oxides provide antireflection coatings, which can help increase absorption in solar cells. Among the II–VI group of semiconductors, zinc oxide (ZnO) has a wurtzite crystal structure, a direct and wide bandgap energy of 3.37 eV, a high exciton binding energy of 60 meV, and a good optical gain at room temperature [1–3]. Wurtzite ZnO is used in a variety of applications, such as field-effect transistors [4], optical components [5], dye-sensitized solar cells [6], and

CB (e¹)

OH
OH
Acid red dye

Weredungh (non)

Antibacterial activity

^{*} Corresponding author: Kommu Jaya Rao, Department of Humanities and Basic Sciences, Welfare Institute of Science Technology and Management, Visakhapatnam-531173, India,

e-mail: jayaraokommu1@gmail.com

^{*} Corresponding author: Malla Ramanaiah, Department of Chemistry, Aditya Institute of Technology and Management, Tekkali-532201, India, e-mail: ramanaiahmalla4@gmail.com

2 — Sattaru Gouthamsri *et al.* DE GRUYTER

solid-state gas sensors [7,8]. Various nanostructured materials are being researched right now to regulate light and enhance absorption in photovoltaic cells. ZnO is a potential material for optoelectronic devices because it possesses a variety of practical electrical and optical aspects. Recent research demonstrates that the defect centres and defect concentrations found in the ZnO lattice can regulate the optical, magnetic, and electrical properties of ZnO nanostructures [9,10]. Due to its comparable ionic radius, many electronic states, and divalent state, cobalt is a desirable transition metal for doping ZnO. Additionally, cobalt-doped ZnO samples have remarkable optical and magnetic properties even at low concentrations of cobalt substitution [11,12]. Sputtering, sol-gel, spin coating, solvothermal, ultrasonic spray, and pulsed laser deposition processes have all been used to create cobalt-doped ZnO thin films and nanostructures [13-17].

Doping with transition metals like chromium, vanadium, iron, and cobalt has also been investigated as a way to increase its photoactivity and broaden its spectrum response. Transition metals may function as shallow traps in the lattice ZnO, which would prevent photoinduced electron-hole pairs from recombining on a photocatalyst's surface. The presence of secondary phases, such as Co³⁺ ions, which may coexist with Co²⁺ ions, is expected to have lattice defects in cobalt-doped ZnO nanohybrids. Cobalt-doped ZnO is therefore considered to be a possible choice among the transition metal in diluted magnetic semiconductors because of its abundant electron states, high solubility in the ZnO matrix, and similar ionic radius (0.58 Å) to that of Zn (0.6 Å) [18]. The photocatalytic proficiency of the synthesized catalyst was observed by visible light-induced degradation of acid red (AR) dye. AR dye is mostly used as a colouring agent in the leather and textile industries; this industrial effluent is crucial owing to its high toxicity, solubility in water, relative environmental stability, and potential for health issues [19,20]. The same photocatalytic approach was implemented for treating pathogenic bacteria, such as Gram +ve bacteria (Spingomonous pausimobilis) and Gram –ve bacteria (Streptococcus pyrogenes), which cause skin infections in human beings. Hence, cobalt-doped ZnO (Co/ZnO) nanohybrid was proposed for this study based on the aforementioned advantages for catalytic and antimicrobial activities.

2 Experimental details

2.1 Materials

Without further purification, the desirable solutions were made using double distilled water, and all the compounds used in the synthesis were of the analytical grade. Zinc acetate $\text{Zn}(\text{CH}_3\text{COO})_2$ and cobalt chloride (CoCl_2) were obtained from E-Merck (Germany); ethylene glycol, HNO_3 , and glycine were obtained from Himedia, India. The AR dye was obtained from Himedia, India, and utilized as a model dye pollutant. The microorganisms were received from IMT Chandigarh, India.

2.2 Synthesis of Co/ZnO nanohybrid

In order to synthesize Co/ZnO nanohybrid in wt% (ZnO_{0.6} CO_{0.4}), 20 mL of CoCl₂ was combined with 20 mL of ethylene glycol and 3.2 mL of HNO₃ in a 150 mL Pyrex glass beaker (solution-I) with glycine as a fuel for combustion. The mixture was stirred for 15 min. The required weight% of Zn (CH₃CO₂)₂·2H₂O, 20 mL of 1,2-ethanediol, and 3.5 mL of deionized water were added to another beaker for the hydrolysis process (solution II). Solution I was vigorously mixed as Solution II was added drop by drop. A colloidal suspension was formed after solution II was fully added. This suspension was then stirred for an additional 90 min and kept in storage for 48 h. The final product was washed with water several times and dried in an oven for 8 h.

2.3 Instrumentation

Several instrumental techniques were used to analyse the crystalline size, pure phase, optical properties, morphology, thermal stability, and functional groups of the prepared materials. These included XRD (Bruker, Cu- K_{α} radiation in the 2θ range from 10° to 80° at a scanning rate of 2° /min), FTIR (IR Prestige 21, scan from $400-4,000~\text{cm}^{-1}$), and SEM (JEOL JSM-6700F). UV-Vis diffused reflectance spectra were recorded (Shimadzu, 2600R, wavelength scan range of 200–800 nm with BaSO₄ as reference). Thermal analyses (TGA) were achieved in N_2 atmosphere with a heating rate of 10° C/min using a Perkin-Elmer model 4000 instrument. Multipack 6.0A software was used to evaluate the fitting of XPS curves. The surface area and pore volume of the samples were calculated using the Brunauer–Emmett–Teller (BET) surface area analyser (model: Gemini VII 2390 series micro metrics).

2.4 Evaluation of photocatalytic performance

The photocatalytic performance of the prepared Co/ZnO nanohybrid was determined by the photocatalytic degradation of the dye pollutant AR under visible light illumination. The photoreactor used in this study consisted of a

380 W metal halide lamp with a 570 nm cut-off filter. In the beginning, 50 mL of an aqueous AR dye solution was mixed with 0.05 g of precalculated photocatalyst, and the mixture was kept in a water-cooling beaker and stirred for 30 min in dark conditions to achieve adsorption-desorption thermal equilibrium. After 30 min, the reaction beaker was exposed to the necessary quantity of light, and the samples were collected in prescribed vials at regular time intervals and measured using a UV-Vis spectrometer. The photocatalytic degradation efficiency (% DE) was determined by the following equation:

% DE =
$$A_0 - A_t/A_0 \times 100$$
, (1)

where A_0 is the initial dye absorbance and A_t is the absorbance at time t of the AR dye aqueous solution.

2.5 Antibacterial activity assay

The well diffusion method was used to measure the antibacterial activity of the Co/ZnO nanohybrid against bacterial

strains (S. pausimobilis and S. pyrogenes). The test organisms (18 h-old cultures) were injected with nutrient agar media and put into a Petri plate. The media on the plates were allowed to harden at room temperature. Four wells, each measuring 5 mm in diameter, were drilled onto each plate after the medium had been set. Stock solutions of the test chemical at different concentrations (200, 300, and 400 µg/mL) were made. As a result, sterile micropipettes were used to transfer 50 µg/mL of each concentration into the plate. After completion, the zone of inhibition around the well was measured in millimetres.

3 Results and discussion

3.1 Morphology and XPS analyses

Figure 1 shows the SEM images of the prepared Co/ZnO nanocatalyst. They reveal the size and distribution of the particles in the samples. Figure 1(a) and (b) exhibits the

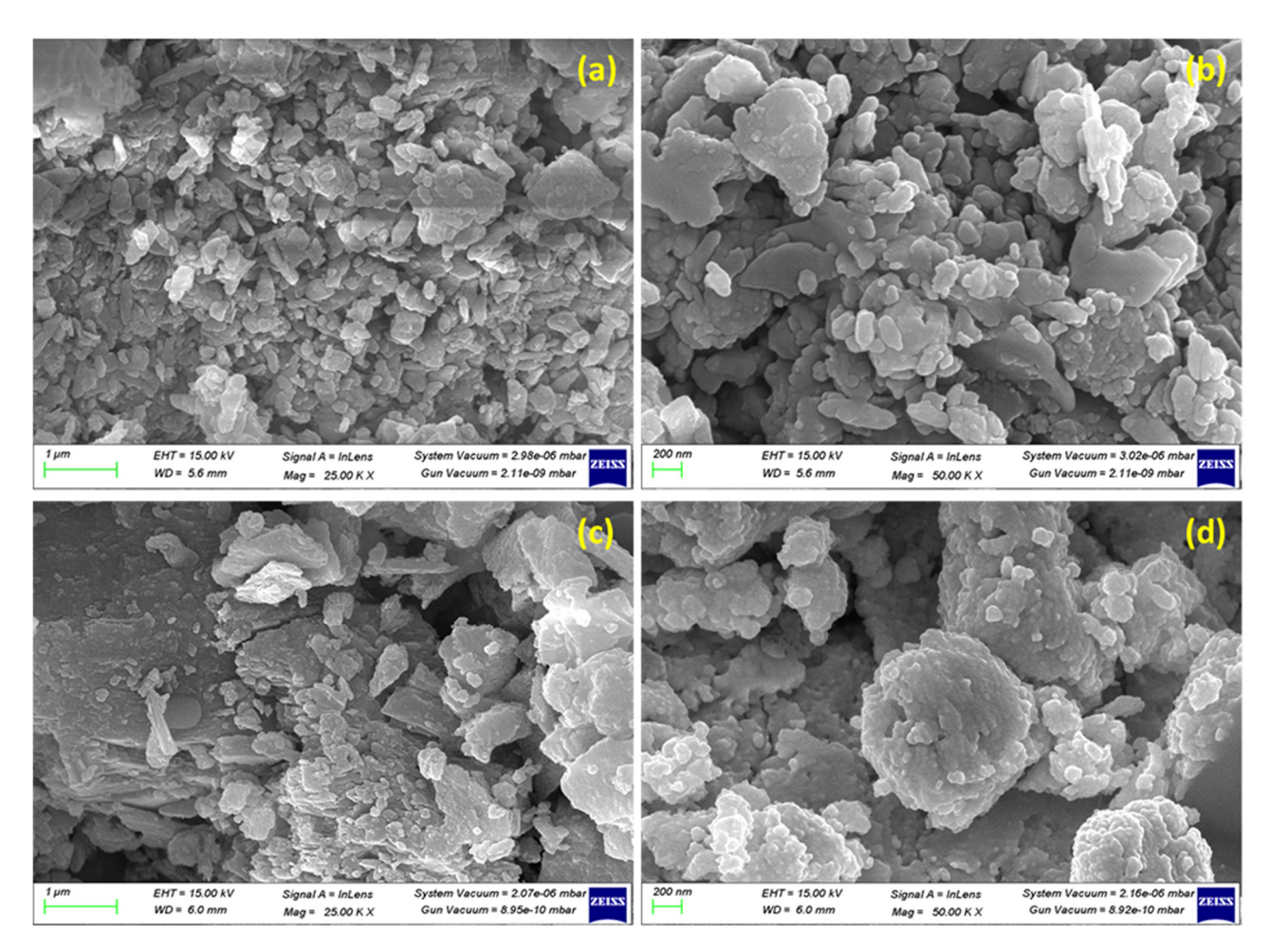


Figure 1: SEM images of (a and b) undoped ZnO and (c and d) Co/ZnO nanohybrid.

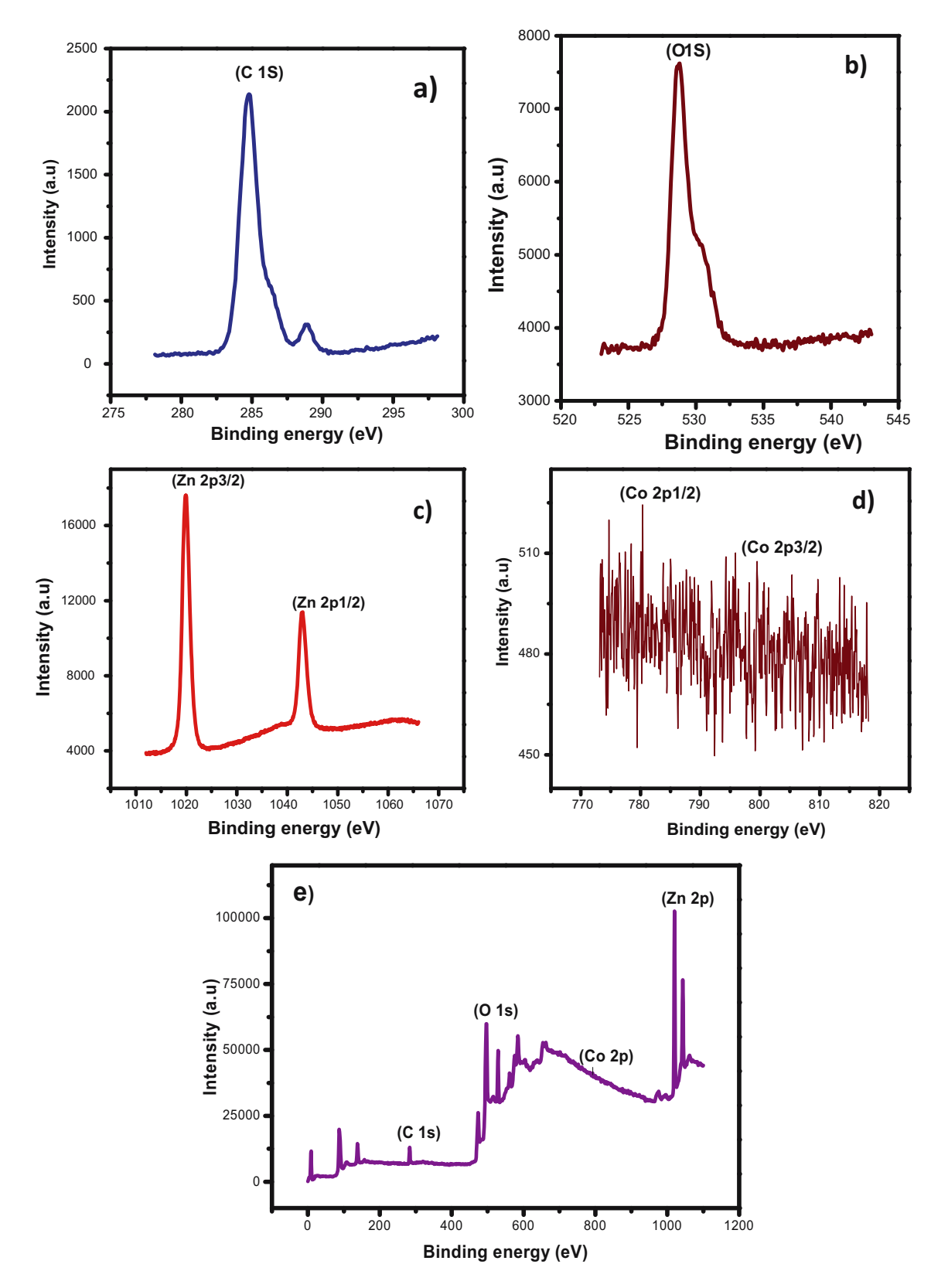


Figure 2: XPS spectra of (a) C 1s, (b) O 1s, (c) Zn 2p, (d) Co 2p. (e) Survey spectrum of the Co/ZnO nanohybrid.

SEM images of the prepared pure ZnO, which are agglomerated with high purity, and the particle size of 39 nm was obtained from imageJ. However, the prepared nanohybrid exhibited a particle size of 31 nm and it was observed that the Co-doped ZnO grain size seems to be more abundant and diverse than that of the undoped ZnO as shown in Figure 1(c) and (d). The SEM images of all prepared samples showed the formation of crystallites of a nanometre in size; however, as the cobalt concentration was increased, there were no appreciable changes in the grain size.

The elemental analysis of the synthesized samples was determined by XPS. The oxidation peaks of Co/ZnO NPs are depicted in Figure 2(a)-(e). The peaks related to binding energies of C, O, Zn, and Co and the survey spectrum of Co/ ZnO were revealed. The binding energies of the two peaks (Zn 2p) at 1020.7 and 1044.1 eV, were attributed to the core levels Zn 2p3/2 and Zn 2p1/2, respectively [21]. The measured energy difference, which agrees with the earlier report, was found to be 23.4 eV. As shown in Figure 2(b), which depicts the system's cobalt valence states, the Co peaks must fit into two Gaussian peaks with various binding energy positions. The binding energies of Co 2p peaks were positioned at 794.4 and 779.2 2p3/2 eV. According to reports, the binding energy difference of Co 2p was 15.2 eV [22]. The O1s' binding energy values were located at 529.22 eV and 530.66 and C 1s binding energies were located at 285 eV. Therefore, Co²⁺ can successfully replace Zn²⁺ in the ZnO lattice, and Co ions in the oxidation state are surrounded by O ions.

Co/ZnO ZnO 10 20 30 40 50 60 70 80 90 2 Theta (degrees)

Figure 3: XRD patterns of prepared ZnO and Co/ZnO nanohybrid.

3.2 XRD and FTIR spectral analysis

Co-doped ZnO and ZnO with XRD patterns are shown in Figure 3. Undoped ZnO and the Co/ZnO nanohybrid exhibited polycrystalline nature with copious peaks including (100), (002), (102), (110), and (004) planes, which well coincided with the previous report (JCPDS file No. 89-0510). All diffraction peaks are in agreement with the experimental data for a hexagonal ZnO wurtzite structure, demonstrating that doped Co²⁺ ions do not affect the crystal structure. However, as the concentration of Co²⁺ doping increases, the intensity of the diffraction peaks weakens and the halfpeak breadth widens, suggesting that the Co²⁺ ions suppress the growth of ZnO particle aggregation and influence ZnO crystallization [23]. No characteristic cobalt or cobalt oxide peaks were observed in any of the patterns, which may represent that Co²⁺ ions have replaced Zn²⁺ or are present as amorphous particles. Using the Debey-Scherrer equation $(D = k\lambda/\beta\cos\theta)$, the average crystalline sizes (D) of the undoped and Co-doped samples were measured. The doping of cobalt into ZnO was achieved with a lower sample size (21.3 nm) than the pure ZnO (29.6 nm). The lower-size sample may yield better photocatalytic performance over the dye pollutants and pathogens.

FTIR analysis was employed in this study to examine the prepared doped and undoped ZnO and quality. Figure 4 displays the FTIR spectra of cobalt-doped and pure ZnO nanoparticles. The Zn–O bond may be seen in the spectra at around 450–490 cm⁻¹, The band at 490 cm⁻¹ may be

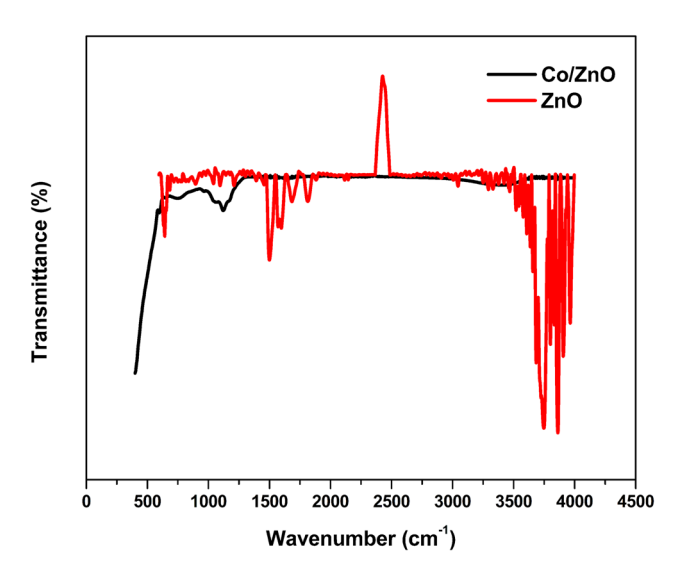


Figure 4: The FTIR spectral image of the prepared ZnO and Co/ZnO nanohybrid.

attributed to oxygen deficit in ZnO. The peaks located at 1,350 cm⁻¹ are related to the ZnO surface's C–O absorption. The carbonate that is represented by the faint absorption band at 2,367 cm⁻¹ likely originates from the ambient CO₂ during the synthesis. The large peaks located at 3,429 cm⁻¹ are attributed to the O–H stretching mode of the hydroxyl groups, and the bending at 1,634 cm⁻¹ is caused by the zinc carboxylate's asymmetrical stretching [24,25]. The peak transmittance percentage in cobalt-doped ZnO was completely quenched. Together, these findings revealed the imperfections present close to the ZnO surface. The absence of any further peaks in the spectra supports the conclusion that the final products are ZnO nanoparticles.

degradation were demonstrated to take place between 122–154°C and 200–400°C, respectively. The weight dropped by 3.4 and 28.7% in the second and third stages, respectively. The weight decrease in the second stage may be due to the evaporation of the water content. The temperatures between 122 and 154°C and 200 and 400°C were observed to constitute the second and third stages of the breakdown, respectively. The weight loss in the second step, however, is due to the disintegration of the Zn–Co precursor which results in the formation of the Co/ZnO nanohybrid. The calcination temperature of the powders was chosen to be above 400°C because there was no visible difference in the weight loss at that temperature.

3.3 Thermal properties

The Co/ZnO nanohybrid was further subjected to gravimetric (TGA) testing to ascertain the weight loss process and an approximate calcination temperature. The precipitate obtained was washed with deionized water followed by ethanol, and it was dried at 100°C. The TGA curve of Co/ZnO nanoparticles is shown in Figure 5. Under a nitrogen environment, the synthesized catalyst was heated at a rate of 10°C/min until it reached 1,000°C. This suggests an 8.7% weight decrease, which might be the result of ethanol evaporation. The two subsequent phases of the

3.4 Surface area and bandgap energy

Figure 6 shows the results of BET analysis, which was used to determine the surface area of ZnO and Co-doped ZnO nanoparticles prepared by sol–gel combustion. At high relative pressures ($P/P_{\rm o}$), the non-limiting adsorption of the catalysts is characteristic of the H3 loop type, which indicates the presence of mesoporous and macroporous structures. As shown in Table 1, the BET surface area of the Co/ZnO nanohybrid is 84 m²/g, which is higher than that

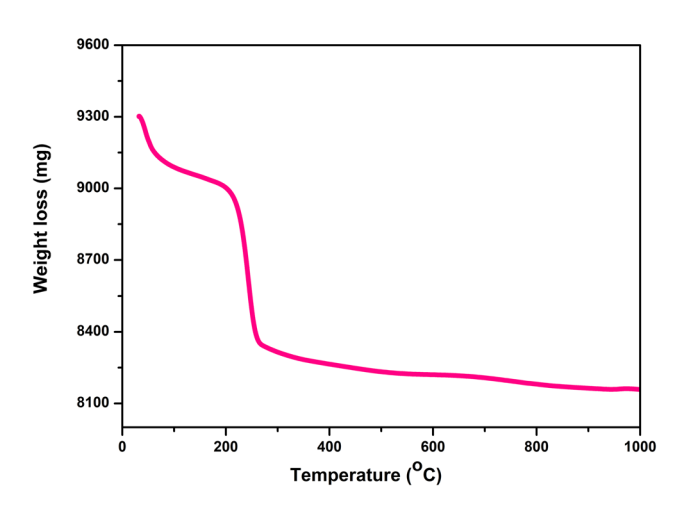


Figure 5: Thermogram curve of the prepared Co/ZnO nanohybrid.

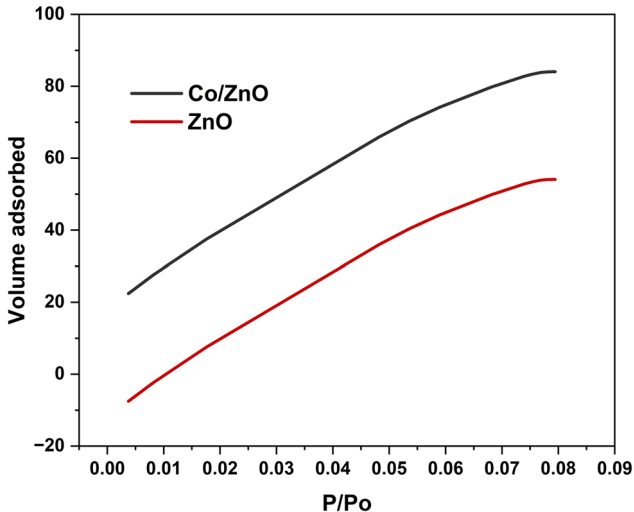


Figure 6: Sorption isotherms of the prepared samples.

Table 1: Properties of the prepared samples

Sample name	Particle size (nm)	Crystalline size (nm)	Surface area (m²/g)	Bandgap energy (eV)
ZnO	39	29.6	53	3.06
Co/ZnO	31	21.3	84	2.4

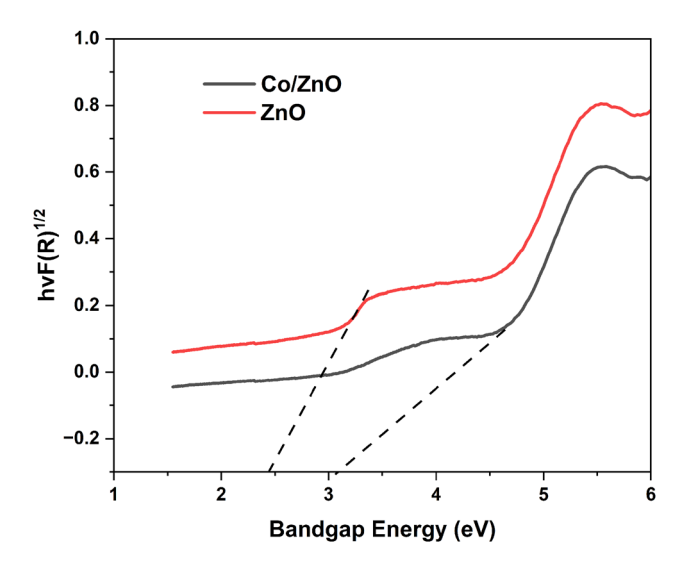


Figure 7: UV-DRS spectral analysis of the prepared samples.

of pure ZnO (53 m²/g). This is due to the doping of cobalt into ZnO, which increases the number of active sites on the surface of the nanoparticles. The higher surface area of the Co/ZnO nanohybrid allows it to accommodate more dye molecules, which leads to a higher degradation rate.

Figure 7 shows UV-visible diffuse reflectance spectra (DRS) of the prepared ZnO and Co/ZnO nanohybrid via the sol–gel approach supported by the combustion process. The optical properties (bandgap energy in eV) of the prepared samples were examined by using the Tauc plot:

$$\alpha h v = A[h v - E_g] n/2. \tag{2}$$

The analysis results indicate that the prepared nanohybrid (Co/ZnO) exhibits lower bandgap energy (2.4 eV) than the pure ZnO (3.06 eV), as presented in Table 1. The lower bandgap energy material shows greater photocatalytic performance towards the degradation of AR dye.

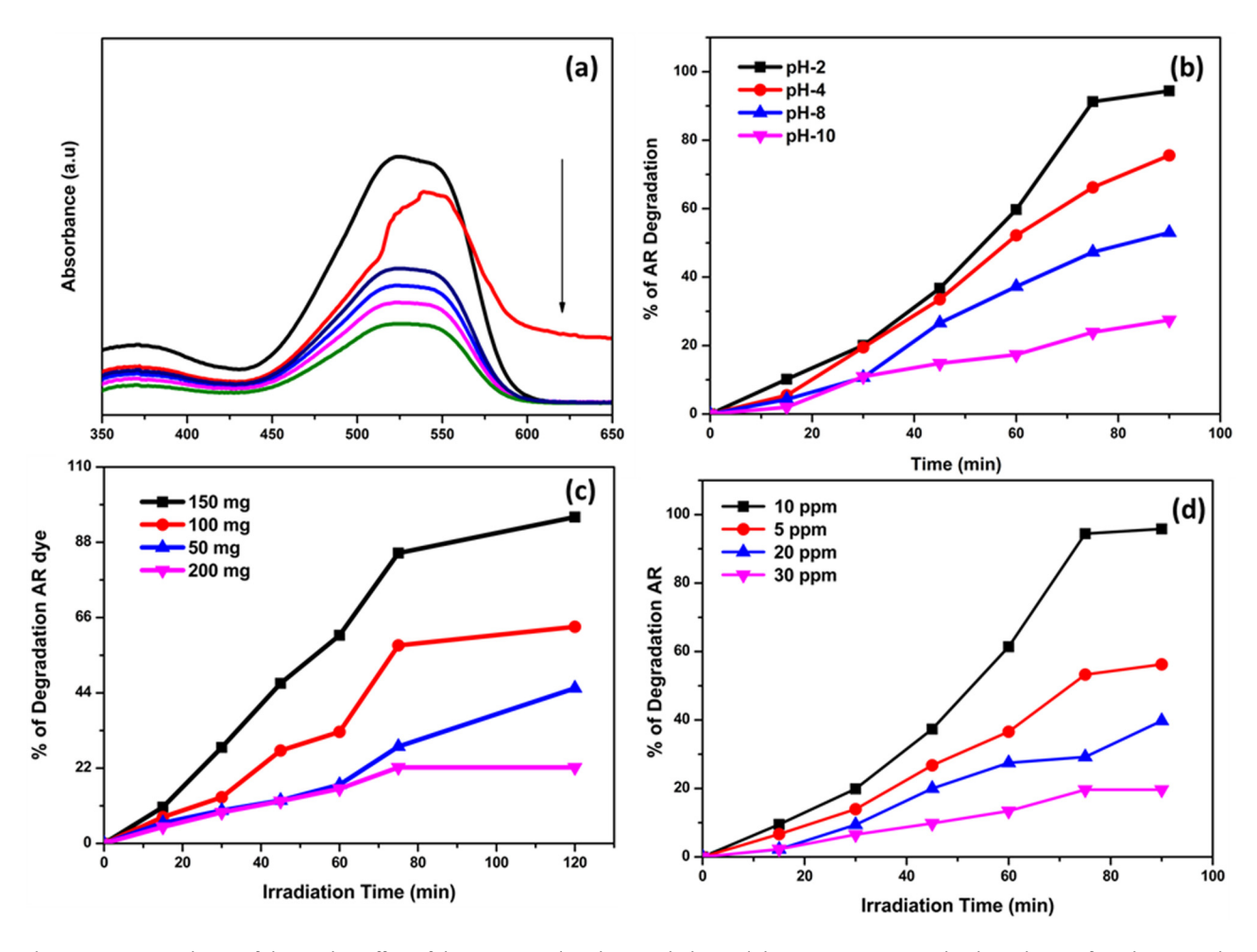


Figure 8: (a) Degradation of the AR dye. Effect of (b) pH, (c) catalyst dose, and (d) initial dye concentration on the degradation of AR dye using the Co/ZnO nanohybrid.

8 — Sattaru Gouthamsri et al. DE GRUYTER

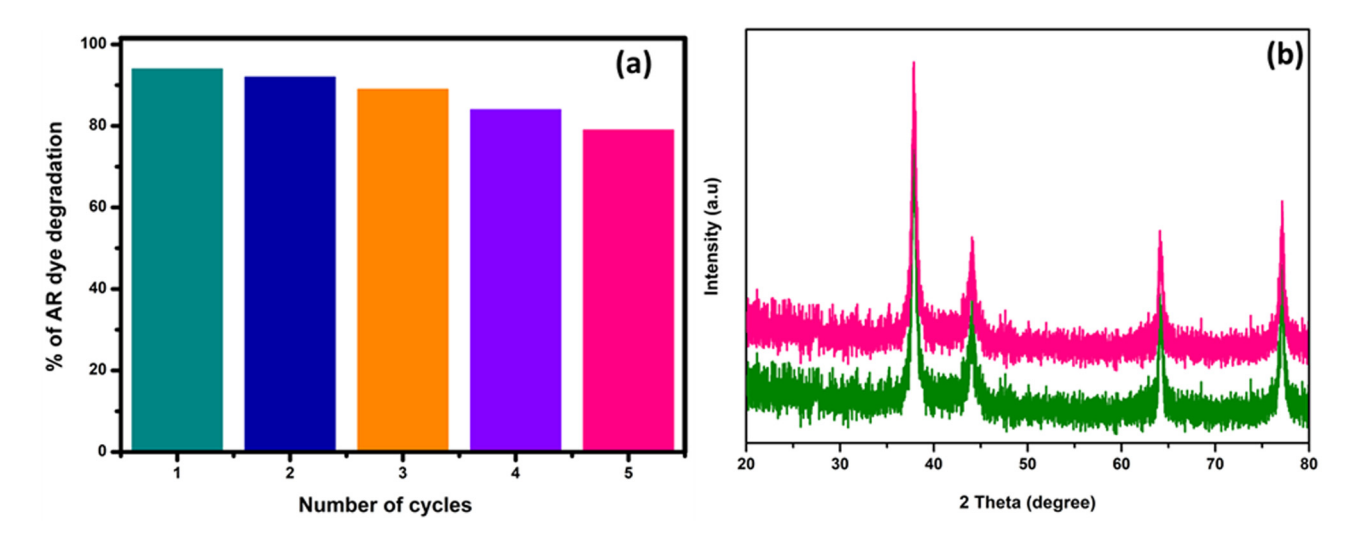


Figure 9: Recyclability (a) and sustainability (b) of the Co/ZnO nanohybrid.

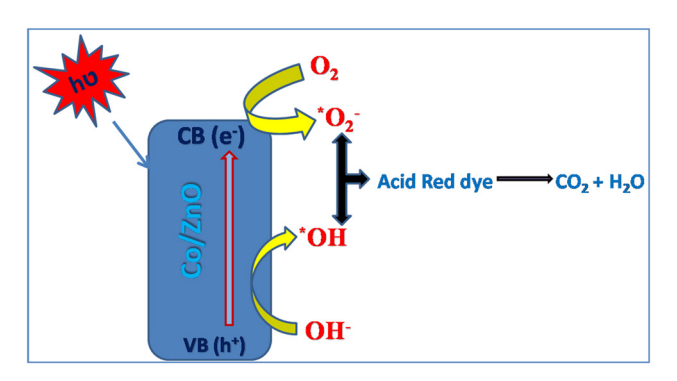


Figure 10: Possible mechanism for photocatalytic degradation of the AR dve.

3.5 Photocatalytic degradation of the AR dye

Figure 8a shows the photocatalytic performance of the prepared Co/ZnO nanohybrid as a suitable photocatalyst for the decolourization of the AR dye under visible light irradiation. A lower photodegradation rate was observed when pure ZnO was used (48% in 200 min). As expected, the degradation rate was increased with the Co/ZnO nanohybrid at similar conditions. These results lead to further examination of optimized conditions for complete degradation of the AR dye under visible light irradiation. By changing the target parameter while keeping the other parameters constant, the effects of the reaction parameters such as pH, catalyst dose, and initial dye concentrations were examined to reach the maximum photodegradation rate of the AR dye.

3.5.1 Optimization conditions

Because of the effect of the electrostatic interactions between the catalyst surface (Co/ZnO), AR dye, and charged radicals, the pH of the solution is an important variable parameter in the evaluation of the photocatalytic dye degradation efficiency of the catalyst in an aqueous medium. Using the prepared Co/ZnO catalyst, the impact of pH on the percentage degradation of the AR dye when exposed to visible light was determined. The results are shown in Figure 8b. It can be seen from the figure that in acidic media as opposed to the basic medium, AR degrades at a higher proportion. The negatively charged dye molecules and the positively charged catalyst surface may interact more electrostatically as a result [26]. The catalyst surface develops a -ve charge and repels the same charged dye molecules electrostatically when the pH is increased to a basic medium. The rate of AR degradation was maximum at acidic pH 2. The negatively charged AR can easily adsorb on the catalyst surface.

Figure 8(c) shows the impact of the catalyst dosage on AR degradation. The rate of degradation was calculated by varying the catalyst concentrations (50, 100, 150, and 200 mg) applied to 100 mL of solution containing 10 ppm of dye at pH 2. The rate of degradation increases linearly up to a catalyst loading of 150 mg and then starts to decrease. The catalyst particles may not be activated by light transmission due to an increase in turbidity and agglomeration of the catalyst particles [27], and the catalyst particles may also be deactivated by collisions between

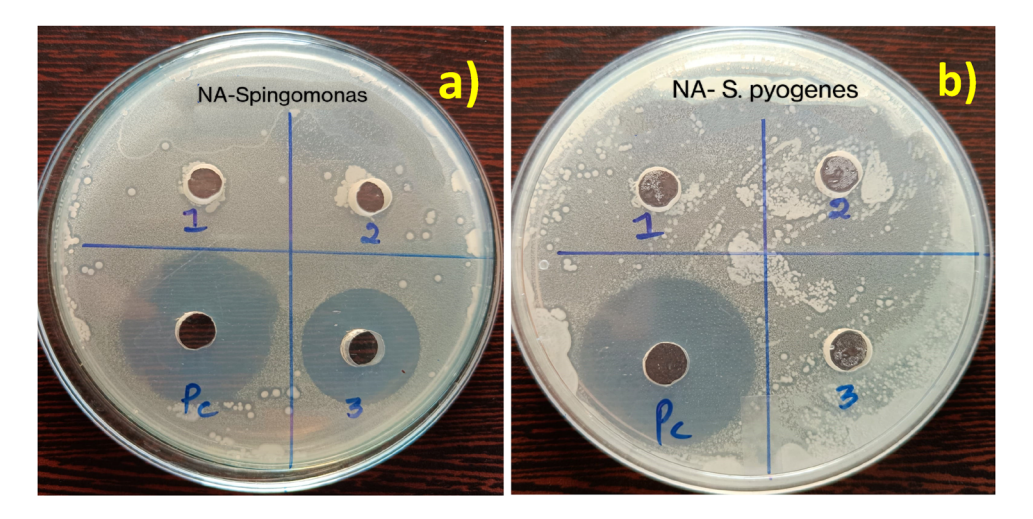


Figure 11: Antibacterial properties of Co/ZnO against (a) S. pausimobilis and (b) S. pyrogenes.

active molecules and the ground state molecules of Co/ZnO [28]. The AR dye at different concentrations ranging from 5 to 30 ppm was used to evaluate the impact of the initial dye concentration (AR) at a fixed catalyst weight (150 mg) and pH 2. The rate of AR dye degradation increased up to 20 ppm, as shown in Figure 8(d). However, if the dye concentration is increased further, the catalyst will become inactive due to the blanket effect, and the rate of degradation decreases [29].

3.5.2 Recyclability and sustainability

The catalyst's stability was evaluated by recycling tests that were exposed to visible light. After 120 min, the photocatalytic reaction with Co-doped ZnO was completed. The photocatalyst was then taken from the solution and rinsed with distilled water. The photocatalyst concentration and AR were both maintained constant. Figure 9a demonstrated that even after four cycles, the catalyst's catalytic activity towards the pollutant was still substantial. It was observed that the high degree of repeatability of the photocatalytic activity may be due to the AR dye molecules coating the photocatalyst surface. The Co/ZnO nanocatalyst surface properties and photocatalytic performance are impacted by the extremely challenging nature of cleaning

Table 2: Agar-well diffusion of the Co-doped ZnO nanohybrid over *S. pausimobilis* and *S. pyrogenes*

Organism	200 μg/mL	300 μg/mL	400 μg/mL	Control µg/mL
S. pausimobilis S. pyrogenes	_	_	16 mm —	23 mm 25 mm
s. py. ogenes				

the synthesized catalyst surface. The combustion-supported sol—gel approach is fascinating for the better photocatalytic performance of the Co/ZnO nanohybrid over AR dye under visible light irradiation and stable for successive five runs without maximum loss as shown in Figure 9b. This is evident from the XRD patterns that are the same compared to that of the fresh ones.

3.5.3 Possible mechanism

Based on the results of previous experiments [30], a simple and feasible mechanism for the oxidative photocatalytic degradation of AR dye under Co/ZnO nanohybrid illumination is provided (Figure 10). For this reason, ZnO was first exposed to photon energy from visible light, and then electrons moving to the conduction band (CB) and holes (h^+) were produced in the valence band. Hydroxyl radicals (OH), which react with an aqueous solution, are formed when h^+ interacts with it. Superoxide radicals (O_2) are generated when the excited electron in CB interacts with oxygen molecules. Radicals, also known as reactive oxygen species, are mostly responsible for degrading the AR dye into non-biodegradable elements like water and carbon dioxide.

3.5.4 Antibacterial performance

The prepared Co/ZnO nanohybrids were further examined for their antibacterial properties on *S. pausimobilis* and *S. pyrogenes* using the well diffusion method [30]. Various concentrations of Co/ZnO nanoparticles were placed in different wells of a Petri dish at standard concentrations of 200 µg/mL (1), 300 µg/mL (2), and 400 µg/mL (3) along with

chloramphenicol as a positive control (4). Figure 11 shows the antibacterial performance of the prepared Co/ZnO nanohybrid. The diameter of the bacterial growth zone was calculated and is shown in Table 2. The results of the activity tests revealed that there is no activity observed in *S. pyrogenes*, but the optimal concentration of Co/ZnO for the zone of inhibition of *S. pausimobilis* (400 μ g/mL) is also very nearer to the reference value; Co/ZnO nanoparticles have good antibacterial activity. The electron—hole formation that occurs in the valance band of ZnO after the catalyst is exposed to visible light may be the cause of this inhibition. This e^-/h^+ , positive hole functions as a strong oxidizing agent under visible light, which could destroy the protein coat of the bacteria and inhibit its growth.

4 Conclusion

Cobalt-doped ZnO nanohybrids were synthesized by the combustion-supported sol-gel method at various concentrations. At 400°C, the synthesized nanoparticles were all annealed. The particle size grows as the concentration of cobalt dopant increases. The obtained Co/ZnO nanoparticles exhibit high photocatalytic performance over the degradation of AR dye when exposed to visible light. Photodegradation performs well at lower pH levels from the photodegradation experiment results. When visible light is introduced to the dye solution, the photodecolorization process accelerates within 120 min. The Co/ZnO nanohybrid was the most effective for S. pausimobilis. The experimental results conclude that Co/ZnO acts as a better photocatalyst for AR dye degradation under visible light irradiation and antibacterial performance. The prepared Co/ZnO nanohybrid showed an increase in photocatalytic activity upon illumination and acts as a benign catalyst for the degradation of AR dye and antimicrobial resistance for a few pathogens.

Acknowledgement: The authors express their gratitude to Bio Enviro Chemical Solutions, Visakhapatnam, for providing an instrumentation facility.

Funding information: No financial support.

Author contributions: Sattaru Gouthamsri and Malla Ramanaiah: Formal analysis, methodology, data interpretation, writing-original draft; Kommu Jaya Rao and Keloth Basavaiah: Writing-review & editing.

Conflict of interest: The authors declare that there were no conflicts of interest.

Ethical approval: The conducted research is not related to either human or animal use.

Data availability statement: The data will be provided by mail request to the corresponding author.

References

- Klingshirn C. ZnO: From basics towards applications. Phys Stat Sol. B. 2007;244:3027–73.
- [2] Wong E, Searson P. ZnO quantum particle thin films fabricated by electrophoretic deposition. Appl Phys Lett. 1999;74:2939.
- [3] Vispute RD, Huuavarad SS, Pugel DE, Kulkami VN, Dhar S, Takeuchi I, et al. Wide band gap ZnO And ZnMgO heterostructures for future optoelectronic devices. In: Thin Films and Heterostructures for Oxide Electronics. Multifunctional Thin Film Series. Berlin Heidelberg New York: Springer; 2005. p. 301–30.
- [4] Wang XD, Zhou J, Song JH, Liu J, Xu N, Wang ZL. Piezoelectric field effect transistor and nanoforce sensor based on a single ZnO nanowire. Nano Lett. 2006;6:2768–72.
- [5] Yang PD, Yan HQ, Mao S, Russo R, Johnson J, Saykally R, et al. Controlled growth of ZnO nanowires and their optical properties. Adv Funct Mater. 2002;12:323–31.
- [6] Law M, Greene LE, Johnson JC, Saykally R, Yang PD. Nanowire dyesensitized solar cells. Nat Mater. 2005;4:455–9.
- [7] Navale SC, Gosavi SW, Mulla Talanta IS. Controlled synthesis of ZnO from nanospheres to micro-rods and its gas sensing studies. Talenta. 2008;75:1315–9.
- [8] Zhang J, Wang S, Wang Y, Xu M, Xia H, Zhang S, et al. ZnO hollow spheres: Preparation, characterization, and gas sensing properties. Sens Actuators B. 2009:139:411–7.
- [9] Jin Z, Fukumura T, Kawasaki M, Ando K, Saito H, Sekiguchi T, et al. High throughput fabrication of transition-metal-doped epitaxial ZnO thin films: a series of oxide-diluted magnetic semiconductors and their properties. Appl Phys Lett. 2001;78:3824–6.
- [10] Simimol A, Anappara AA, Barshilia HC. Influence of defects on electrical properties of electrodeposited co-doped ZnO nanocoatings. Mater Res Express. 2017;4:015001.
- [11] Simimol A, Anappara AA, Greulich-Weber S, Chowdhury P, Barshilia HC. Enhanced room temperature ferromagnetism in electrodeposited Co-doped ZnO nanostructured thin films by controlling the oxygen vacancy defects. J Appl Phys. 2015;117:214310.
- [12] El Mir L, Ben Ayadi Z, Rahmouni H, El Ghoul J, Djessas K, von Bardeleben HJ. Elaboration and characterization of Co doped, conductive ZnO thin films deposited by radio-frequency magnetron sputtering at room temperature. Thin Solid Films. 2009;517:6007–11.
- [13] Ahmed F, Kumar S, Arshi N, Anwar MS, Koo BH, Lee CG. Doping effects of Co²⁺ ions on structural and magnetic properties of ZnO nanoparticles. Microelectron Eng. 2012; 89:129–32.
- [14] Gu H, Zhang W, Xu Y, Yan M. Effect of oxygen deficiency on room temperature ferromagnetism in Co doped ZnO. Appl Phys Lett. 2012;100:202401.
- [15] Pal B, Dhara S, Giri PK, Sarkar D. Room temperature ferromagnetism with high magnetic moment and optical properties of Co doped ZnO nanorods synthesized by a solvothermal route. J Alloy Compd. 2014;615:378–85.

- [16] Al-Toriahi AKM, Azooz EA, Al-Mulla EAJ. Metal nanoparticles and nano-filters for the disposal of hospital waste: a review. Nano Biomed Eng. 2023;15(2):179–90.
- [17] Taddesse AM, Bekele T, Diaz I, Adgo A. Polyaniline supported CdS/ CeO₂/Ag₃PO₄ nanocomposite: An "A-B" type tandem n-n heterojunctions with enhanced photocatalytic activity. J Photochem Photobiol A: Chem. 2021;406:113005.
- [18] Carvalho HB, Godoy MPF, Paes RWD, Mir M, Zevallos FAO, Iikawa MJSP, et al. Absence of ferromagnetic order in high quality bulk Co-doped ZnO samples. Appl Phys. 2010;108:033914–9.
- [19] Kenawy E-R, Ghfar AA, Wabaidur SM, Khan MA, Siddiqui MR, Alothman ZA, et al. Cetyltrimethylammonium bromide intercalated and branched polyhydroxystyrene functionalized montmorillonite clay to sequester cationic dyes. J Environ Manag. 2018;219:285–93.
- [20] Othman ZAA, Wabaidur SM. Application of carbon nanotubes in extraction and chromatographic analysis: a review. Arab J Chem. 2019;12(5):633–51.
- [21] Kwon YJ, Kim KH, Lim CS, Shim KB. Characterization o fZnO nanopowders synthesized by the polymerized complex method via an organochemical route. J Ceram Proc Res. 2002;3:146–9.
- [22] Lakshmi YK, Srinivas K, Sreedhar B, Raja MM, Vithald M, Reddy PV. Structural, optical, and magnetic properties of nanocrystalline Zn0.9Co0.10-based diluted magnetic semiconductors. Mater Chem Phys. 2009;113:749–55.
- [23] Bouloudenine M, Viart N, Colis S, Dinia A. Bulk Zn1–xCoxO magnetic semiconductors prepared by hydrothermal technique. Chem Phys Lett. 2004;397:73–6.

- [24] Kenawy E-R, Ghfar AA, Wabaidur SM, Ali Khan MA, Raza Siddiqui MR, Alothman ZA, et al. Cetyltrimethylammonium bromide intercalated and branched polyhydroxystyrene functionalized montmorillonite clay to sequester cationic dyes. J Environ Manag. 2018;219:285–93.
- [25] Liu H, Yang D, Sun H, Zhu Z. Microwave assisted hydro-thermal synthesis and characterization of hierarchical structured ZnO nanorods. J Optoelectron Adv Mater. 2010;12:2063–8.
- [26] Rauf MA, Salman Ashraf S. Fundamental principles and application of heterogeneous photocatalytic degradation of dyes in solution. Chem Eng J. 2009;151:10–8.
- [27] Chen CC. Degradation pathways of ethyl violet by photocatalytic reaction with ZnO dispersions. J Mol Catal A: Chem. 2007;264:82–92.
- [28] Kusvuran E, Gulnaz O, Irmak S, Atanur OM, Yavuz HI, Erbatur O. Comparison of several advanced oxidation processes for the decolourization of reactive red 120 azo dye in aqueous solution. I Hazard Mater B. 2004;109:85–93.
- [29] Divya Lakshmi KV, Siva Rao T, Swathi Padmaja J, Manga Raju I, Abdul Alim SK, Kalyani P. Visible light driven mesoporous Mn and S co-doped TiO₂ nano material: characterization and applications in photocatalytic degradation of indigocarmine dye and antibacterial activity. Environ Nanotechnol Monit Manag. 2018;10:494–504.
- [30] Botsa SM, Kumar YP, Basavaiah K. Facile simultaneous synthesis of tetraaniline nanostructures/silver nanoparticles as heterogeneous catalyst for the efficient catalytic reduction of 4-nitrophenol to 4-aminophenol. RSC Adv. 2020;10(37):22043–53.